Quadrature Spatial Modulation for 5G Outdoor Millimeter–Wave Communications: Capacity Analysis

Abdelhamid Younis, Nagla Abuzgaia, Raed Mesleh and Harald Haas

***Abstract*—Capacity analysis for millimeter–wave (mmWave) quadrature spatial modulation (QSM) multiple-input multiple-output (MIMO) system is presented in this paper. QSM is a new MIMO technique proposed to enhance the performance of conventional spatial modulation (SM) while retaining almost all its inherent advantages. Furthermore, mmWave utilizes a wide-bandwidth spectrum and is a very promising candidate for future wireless systems. Detailed and novel analysis of the mutual information and the achievable capacity for mmWave–QSM system using a 3D statistical channel model for outdoor mmWave communications are presented in this study. Monte Carlo simulation results are provided to corroborate derived formulas. Obtained results reveal that the 3D mmWave channel model can be closely approximated by a log–normal fading channel. The conditions under which capacity can be achieved are derived and discussed. It is shown that the capacity of QSM system can be achieved, by carefully designing the constellation symbols for each specific channel model.**

***Index Terms*—Quadrature Spatial Modulation (QSM), Millimeter–Wave (mmWave), Capacity Analysis.**

I. Introduction

Millimeter–wave communication offers a plentiful frequency spectrum, ranging from $30 - 300$ GHz, that can be exploited to achieve multigigabits per second data rates [1–3]. For example the E–band at $70/80$GHz offers 1 Gb/s up to 10 Gb/s for typical distances of 3 km with an available worldwide low cost license [4]. Moreover, it has been shown in [4–7] that wave propagation at E–band has negligible atmospheric attenuation (less than 0.5 dB/km), and is unaffected by dust, snow, and any other channel deterioration. Although heavy rain is shown to significantly impact the performance of E–band mmWave systems. However, heavy rain usually occurs in limited part of the world [8] and the radio link can be designed to overcome the attenuation resulted from heavy rain [4]. Several recent standards have been developed based on mmWave technology including mmWave WPAN (IEEE 802.15.3c-2009) [9], WiGig (IEEE 802.11ad) [10], and WirelessHD [11].

Multiple–Input Multiple–Output (MIMO) systems are one of the most promising technical advances in wireless communications in recent years. Such systems facilitate high–throughput transmission in various recent standards including LTE, WIMAX, and others [12, 13]. Hence, combining mmWave with MIMO systems promises significant boost in the overall achievable data rate to support future generations of broadband wireless communication technologies such as 5G and beyond.

Space Modulation Techniques (SMT) [14, 15], such as spatial modulation (SM) [16, 17], differential spatial modulation (DSM) [18–20], generalized spatial modulation (GSM) [21, 22], and quadrature spatial modulation (QSM) [23, 24], are hybrid MIMO and digital modulation techniques that uses the multiple antennas at the transmitter in a unique way to achieve spatial multiplexing gains. The index of the transmit–antennas represent spatial constellation points that are used to carry additional information bits. QSM is an SMT technique reported recently aiming at overcoming a major criticism of SM [25] and space shift keying (SSK) [26], where data rate enhancement is proportional to the base–two logarithm of the number of transmit antennas. In QSM the *spatial symbols* are expanded to in–phase and quadrature components. One component transmits the real part of a *constellation symbol* and the other one transmits the imaginary part of the *constellation symbol* [24, 27]. In conventional SM, the two parts are transmitted from single transmit antenna to avoid inter–channel interference (ICI) at the receiver input [16]. However and as shown in [24], QSM system avoids ICI as well, since the two transmitted data are orthogonal and modulated on the real part and the imaginary part of the carrier signal. At the same time, an additional base–two logarithm of the number of transmit antennas bits can be transmitted in QSM as compared to conventional SM system.

The QSM idea and its performance over Rayleigh fading channel are presented in [24] and the impact of imperfect channel knowledge at the receiver is studied in [27]. QSM performance over Nakagami-m fading channel is studied in [28]. Also, the expansion of sub-carrier index modulation OFDM system using QSM idea is presented in [29].

Capacity analysis of SM and SSK systems has been considered in previous literature [30–35]. In all previous studies

Abdelhamid Younis and Nagla Abuzgaia are with the University of Benghazi, Electrical and Electronics Engineering Department, Faculty of Engineering, P.O. Box: 7051 Benghazi, Libya (e–mail: {a.alhassi, nagla.abuzgaia}@uob.edu.ly).

Raed Mesleh is with the German Jordanian University, Communications Engineering Department, School of Computer Engineering and Information Technology, Amman Madaba Street, P.O. Box 35247, Amman 11180 Jordan (e–mail: raed.mesleh@gju.edu.jo).

Harald Haas is with The University of Edinburgh, College of Science and Engineering, Institute for Digital Communications, King's Buildings, Mayfield Road, Edinburgh, EH9 3JL, UK (e–mail: h.haas@ed.ac.uk).

when obtaining the capacity, only the constellation symbols are considered in the maximization of the mutual information. However, in space modulation techniques both spatial symbols and constellation symbols carry information [36]. Thus, the maximization of the mutual information must be carried over both spatial symbols and constellation symbols. In this paper, the capacity of QSM system over 3D mmWave outdoor channel is studied, and the capacity is derived by maximizing the mutual information over both spatial symbols and constellation symbols. Obtained results reveal that QSM can achieve the channel capacity, even though QSM has only one data stream. This is unlike spatial multiplexing systems where the number of independent data streams required to achieve the capacity should equal the minimum number among transmit and receive antennas [37]. Furthermore, it is concluded in earlier publications [30–35] that space modulation systems capacity depends on the channel type and can be achieved if the signal constellation follows a complex Gaussian distribution, similar to conventional MIMO systems [38]. However, it is shown in this article that QSM capacity in particular, and space modulated systems in general, can be achieved with proper design of the constellation symbols for the specific nature of the fading channel statistics; such that the resultant of the constellation symbols passing through the channel follows a complex normal distribution.

The use of mmWave MIMO technologies require careful design of propagation characteristics of radio signals. mmWave signals propagate in line of sight (LOS) environment and do not penetrate solid materials very well. Previous studies on mmWave outdoor channel modeling proved that the channel can be safely modeled as LOS or near LOS links [39–44]. Recently, the performance of SSK system over LOS mmWave channel is presented [45]. The pioneering work of the NYU Wireless Lab aims at 3D modeling of the mmWave channel [2, 3, 46–48]. The proposed 3D channel models are comprehensive and fits the conducted measurements. As such, the 3D mmWave channel model proposed in [3] is adopted in this study and detailed and novel capacity analysis of mmWave QSM MIMO system are reported.

Furthermore, the 3D channel model is fitted to a log–normal fading channel with uniform phase distribution. Using capacity and average bit error ratio (ABER) analysis, it is revealed that a log–normal fading channel can closely approximate the 3D mmWave channel model.

In summary and with reference to existing literature, the main contributions of this paper are four folds:

1- Capacity analysis for mmWave–QSM system is discussed and analyzed;
2- System parameters required to achieve capacity are investigated and discussed;
3- Detailed analytical and simulation results over 3D statistical channel model for mmWave outdoor mobile communications are provided and interpreted;
4- A log–normal fading channel is shown to closely approximate the 3D statistical mmWave channel model.

The remainder of this paper is organized as follows: In Section II, the QSM modulator, the channel model, and the maximum–likelihood (ML)–optimum receiver are discussed. The capacity of QSM over the 3D mmWave channel model is analyzed and derived in Section III. Finally, the results are presented in Section IV, and the paper is concluded in Section V.

II. System and Channel Models

A. QSM Modulator

In QSM systems, a block of η-bits $\left(\eta = \log_2\left(MN_t^2\right)\right)$ is transmitted at each particular time instant, where M is the size of the constellation diagram, and N_t is the number of transmit antennas. The incoming data bits are divided into three groups according to the following rules [24],

- The first group, containing $\log_2(M)$ bits are used to modulate a symbol $s_i \in \mathcal{S}$, where $\mathcal{S}$ is an M dimensional vector containing all possible constellation symbols. Without loss of generality, quadrature amplitude modulation (QAM) is considered in this paper.
- The other two groups, each containing $\log_2(N_t)$ bits, are used to determine which two transmit antennas to activate. The first $\log_2(N_t)$ bits determine the index $\ell^{\Re}$ of the antenna to transmit the real part of the symbol s_i, $(s_i^{\Re})$. The last $\log_2(N_t)$ bits determine the index $\ell^{\Re}$ of the transmit antenna to transmit the imaginary part of the symbol s_i, $(s_i^{\Re})$.

Note, the spatial symbol is $\mathcal{H}_\ell = [\mathbf{h}_{\ell^{\Re}}, \mathbf{h}_{\ell^{\Im}}]$, and the constellation symbol is $\mathcal{S}_i = \left[s_i^{\Re}; s_i^{\Im}\right]$, where $\mathbf{h}_\ell$ denotes the ℓ^{th} vector of $\mathbf{H}$, and $\mathbf{H}$ is the $N_r \times N_t$ MIMO channel matrix, with N_r being the number of receive antennas.

To further illustrate the principle working mechanism of QSM, an example is given in what follows. Assume a MIMO system with $N_t = 4$ and $4-$QAM modulation is considered. The number of data bits that can be transmitted at one particular time instant is $\eta = \log_2(N_t^2 M) = 6$ bits. Let the incoming data bits be $k = \Big[\underbrace{1\ \ 1}_{\log_2(M)}\ \underbrace{0\ \ 1}_{\log_2(N_t)}\ \underbrace{1\ \ 1}_{\log_2(N_t)}\Big]$. The first $\log_2(M)$ bits $\left[\begin{array}{cc} 1 & 1 \end{array}\right]$, modulate a $4-$QAM symbol, $s_i = +1 - j$, where j is the imaginary unit, $j = \sqrt{-1}$. The symbol s_i is then divided into real and imaginary parts, $s_i^{\Re} = +1$ and $s_i^{\Im} = -j$. The next $\log_2(N_t)$ bits, $\left[\begin{array}{cc} 0 & 1 \end{array}\right]$, modulate the transmit antenna, $\ell^{\Re} = 2$, to transmit $s_i^{\Re} = +1$. The last $\log_2(N_t)$ bits, $\left[\begin{array}{cc} 1 & 1 \end{array}\right]$, modulate another transmit antenna, $\ell^{\Im} = 4$, to transmit $s_i^{\Im} = -j$.

The resultant vectors from the mapping process are coherently added. Hence, the transmitted vector is,

$$\mathbf{x} = \left[\begin{array}{cccc} 0 & +1 & 0 & -j \end{array}\right]^T. \tag{1}$$

The vector, $\mathbf{x}$, is transmitted over an $N_r \times N_t$ mmWave MIMO channel with a transfer function $\mathbf{H}(f)$, and experiences an N_r-dim additive white Gaussian noise (AWGN) $(\mathbf{n})$, with zero mean and variance σ_n^2 (both real and imaginary parts having a double-sided power spectral density equal to $\sigma_n^2/2$).

The received signal is given by:

$$\mathbf{y} = \mathbf{H}\mathbf{x} + \mathbf{n} = \mathcal{H}_\ell \mathcal{S}_i + \mathbf{n}. \tag{2}$$

Note, the signal-to-noise-ratio (SNR) at the receiver input, assuming normalized channel $E_s = \mathrm{E}[\|\mathcal{H}_\ell \mathcal{S}_\imath\|_{\mathrm{F}}^2] = N_r$, is given by $\mathrm{SNR} = E_s/N_0 = 1/\sigma_n^2$, where $\|\cdot\|_{\mathrm{F}}$ is the Frobenius norm.

It is important to note that it is possible to have $\ell^{\Re} = \ell^{\Im}$ depending on the incoming data bits. For instance, in the previous example if the sequence of incoming bits are all "1"s, the transmitted vector will be $\mathbf{x} = \begin{bmatrix} 0 & 0 & 0 & +1-j \end{bmatrix}^T$ and $\ell^{\Re} = \ell^{\Im} = 4$. Also, even in the case that two transmit antennas are active during one time-slot transmission, the inter-channel interference is entirely avoided at the receiver input since the transmitted data are orthogonal representing the in-phase and the quadrature components of the carrier signal. It has been demonstrated in [24, 27] that single radio frequency (RF) chain can be used and the receiver complexity is identical to that of conventional SM system for the same spectral efficiency.

B. 3D mmWave Channel Model

Omni directional antennas operating at mmWave frequencies are considered in this study. The channel impulse response $h_{n_t,n_r}(t)$ for the n_t–th and n_r–th transmit and receive antenna respectively, can be calculated using the double–directional channel model given in [49, 50],

$$h_{n_t,n_r}(t) = \sum_{l=1}^{L} \underset{n_t,n_r}{h^l} a_l e^{j\varphi_l} \delta(t-\tau_l)\, \delta\left(\Theta - \underset{n_t,l}{\Theta}\right) \delta\left(\Phi - \underset{n_r,l}{\Phi}\right), \tag{3}$$

where $\underset{n_t,n_r}{h^l}$ is the l–th subpath complex channel attenuation between the n_t–th and n_r–th transmit and receive antennas respectively, a_l, φ_l and τ_l are the amplitude, phase and absolute propagation delay of the l–th subpath, $\Theta_{n_t,l}$ and $\Phi_{n_r,l}$ are the vectors of azimuth/elevation angle of departure (AOD) and angle of arrival (AOA) for the n_t–th and n_r–th transmit and receive antennas, respectively; and L is the total number of multipath components. Assuming the antenna arrays at both the transmitter and the receiver are uniformly spaced with distance d, and aligned along the z–dimension, the impulse response in (3) can be reduced to,

$$h_{n_t,n_r}(t) = \sum_{l=1}^{L} \underset{n_t,n_r}{h^l} a_l e^{j\varphi_l} \delta(t-\tau_l)\, \delta\left(\theta^z - \underset{n_t,l}{\theta^z}\right) \delta\left(\phi^z - \underset{n_t,l}{\phi^z}\right), \tag{4}$$

where $\theta^z_{n_t,l}$ and $\phi^z_{n_r,l}$ denoting the elevation AOD and AOA for the n_t–th and n_r–th transmit and receive antennas respectively.

From [51] the transfer function of the impulse response in (4) is given by,

$$h_{n_t,n_r}(f) = \sum_{l=1}^{L} \underset{n_t,n_r}{h^l} a_k e^{j\varphi_l} e^{-j\frac{2\pi}{\lambda} d\left(n_t \sin\left(\underset{n_t,l}{\theta^z}\right) + n_r \sin\left(\underset{n_r,l}{\phi^z}\right)\right)} e^{-j2\pi f \tau_l}, \tag{5}$$

where λ is the carrier wavelength.

The values of a_l, φ_l, $\theta^z_{n_t,l}$, $\phi^z_{n_r,l}$, and τ_l in this paper are generated using the 3–D statistical channel model for outdoor mmWave communications derived in [3], where the frequency is 73 GHz, antenna gains are 24.5 dBi, and the distance at each particular time instance is varied equally likely in the range of [60m − 200m] [3].

Furthermore, let $\mathbf{H}^l$ be an $N_r \times N_t$ matrix containing all $h^l_{n_t,n_r}$ complex MIMO channel attenuations, then, from [50],

$$\mathbf{H}^l = \mathbf{R}_{\text{Rx}}^{1/2} \mathbf{H}_{\text{Rician}} \mathbf{R}_{\text{Tx}}^{1/2}, \tag{6}$$

where R_{Tx} and R_{Rx} are the transmitter and receiver correlation matrices respectively, and $\mathbf{H}_{\text{Rician}}$ is a matrix whose elements obey the small–scale Rician distribution with $K = 10$ dB [52]. From [53] the correlation matrices can be calculated by,

$$R_{u,v} = e^{-j\Theta}\left(0.9e^{-|u-v|d} + 0.1\right), \tag{7}$$

where Θ follows a uniform distribution in the range $[-\pi, \pi]$.

C. ML–Optimum Detector

At the receiver, the channel matrix is assumed to be perfectly known, and the transmitted data symbol and spatial symbols are jointly detected using the ML optimal detector as [24],

$$\left[\hat{\ell}, \hat{\imath}\right] = \arg \min_{\mathcal{H}_\ell, \mathcal{S}_\imath} \|\mathbf{y} - \mathcal{H}_\ell \mathcal{S}_\imath\|_{\mathrm{F}}^2. \tag{8}$$

The detected antenna index or indexes, $\hat{\ell}$, along with the index of the transmitted constellation symbol, $\hat{\imath}$, are used to retrieve the original information bits.

III. Capacity Analysis of mmWave–QSM System

The most fundamental questions about existing and future communication system is: What is the maximum possible transmission rate? In this paper, capacity analysis for mmWave–QSM system is conducted to address this question. The analysis considers the specific nature of QSM system where data bits are transmitted through spatial and signal constellation diagrams. It also adheres to the specific nature of mmWave MIMO communication channel. This is unlike existing capacity analysis for SMT in literature, where signal constellation symbols are only considered without addressing transmitted data over spatial symbols [30–35].

By definition, the ergodic capacity is the maximum number of bits that can be transmitted without any errors, and for conventional MIMO systems is given by [54],

$$C = \mathrm{E}_{\mathbf{H}}\left\{\max_{p_{\mathbf{x}}} I(\mathbf{x}; \mathbf{y}|\mathbf{H})\right\}, \tag{9}$$

where the maximization is done over the choice of $p_{\mathbf{x}}$, with $p_{\mathbf{x}}$ being the probability distribution function (PDF) of the transmitted vector $\mathbf{x}$, $I(\mathbf{x}; \mathbf{y}|\mathbf{H})$ is the mutual information between the transmitted vector $\mathbf{x}$ and the received vector $\mathbf{y}$ knowing $\mathbf{H}$, and $\mathrm{E}\{\cdot\}$ is the expectation operator.

In QSM system, and totally different than conventional MIMO systems, the N_t channel vectors are considered as an N_t–sized constellation diagram and used to convey information. As such, QSM modulates information bits in the channel vectors of the two active transmit antennas, $\mathbf{h}_{\ell^{\Re}}, \mathbf{h}_{\ell^{\Im}}$. At the same time, extra information bits are transmitted through the modulated symbol $s_\imath$. Therefore, for QSM the capacity is

defined as,

$$C = \max_{p_{\mathcal{H}_\ell}, p_{\mathcal{S}_i}} I\left(\mathcal{H}_\ell, \mathcal{S}_i; \mathbf{y}\right). \tag{10}$$

An important note in (10) is that there is *no* averaging over the channel matrix $\mathbf{H}$ similar to conventional MIMO systems, or to previous capacity analysis for SMT presented in literature. This is because the different channel vectors of $\mathbf{H}$ convey information. Thus, the maximization in (10) is carried over the PDFs of the spatial and constellation symbols, $p_{\mathcal{H}_\ell}$ and $p_{\mathcal{S}_i}$, respectively. Note, $I\left(\mathcal{H}_\ell, \mathcal{S}_i; \mathbf{y}\right)$ is the mutual information between the transmitted spatial and constellation symbols, $\mathcal{H}_\ell$ and $\mathcal{S}_i$, and the received vector $\mathbf{y}$.

A. Evaluating the Mutual Information

The mutual information, $I(\mathcal{H}_\ell, \mathcal{S}_i; \mathbf{y})$, is the number of bits that can be decoded without errors at the receiver, and is given by,

$$I\left(\mathcal{H}_\ell, \mathcal{S}_i; \mathbf{y}\right) = H\left(\mathbf{y}\right) - H\left(\mathbf{y}|\mathcal{H}_\ell, \mathcal{S}_i\right), \tag{11}$$

where $H(\cdot)$ is the entropy function.

After some algebraic manipulations given in Appendix A, $I\left(\mathcal{H}_\ell, \mathcal{S}_i; \mathbf{y}\right)$ is derived as,

$$\begin{aligned} I\left(\mathcal{H}_\ell, \mathcal{S}_i; \mathbf{y}\right) = &- N_r \log_2(e) \\ &- \mathrm{E}_{\mathbf{y}}\left\{\log_2\left(\mathrm{E}_{\mathcal{H}_\ell, \mathcal{S}_i}\left\{e^{\frac{-\|\mathbf{y}-\mathcal{H}_\ell \mathcal{S}_i\|_{\mathrm{F}}^2}{\sigma_n^2}}\right\}\right)\right\}. \end{aligned} \tag{12}$$

Unfortunately, no closed–form expression is available for the summation in (12) and numerical methods should be used.

B. Capacity

From (11), the capacity for QSM in (10) can be written as,

$$C = \max_{p_{\mathcal{H}_\ell}, p_{\mathcal{S}_i}} \left(H\left(\mathbf{y}\right) - H\left(\mathbf{y}|\mathcal{H}_\ell, \mathcal{S}_i\right)\right). \tag{13}$$

It is important to note that the entropy $H(\mathbf{y}|\mathcal{H}_\ell, \mathcal{S}_i)$, as shown in (26), does not depend on $\mathcal{H}_\ell$ and $\mathcal{S}_i$. Therefore, the maximization in (13) can be reduced to the maximization of $H\left(\mathbf{y}\right)$.

In [55] it is shown that the distribution that maximizes the entropy is the zero mean complex Gaussian distribution $\left(\mathcal{CN}\left(0, \sigma^2\right)\right)$, where σ^2 is the variance. Thus, to maximize the entropy $H\left(\mathbf{y}\right)$, the received vector $\mathbf{y}$ must be a $\mathcal{CN}\left(\mathbf{0}_{N_r}, \sigma_{\mathbf{y}}^2 \mathbf{I}_{N_r}\right)$, where $\sigma_{\mathbf{y}}^2$ is the variance of $\mathbf{y}$, $\mathbf{0}_N$ an N length all zeros vector, and $\mathbf{I}_N$ is an $N \times N$ square identity matrix. Considering the received signal in (2) and assuming white Gaussian noise, $\mathbf{n}$ is $\sim \mathcal{CN}\left(\mathbf{0}_{N_r}, \sigma_n^2 \mathbf{I}_{N_r}\right)$, the received signal is complex Gaussian distributed, $\mathbf{y} \sim \mathcal{CN}\left(\mathbf{0}_{N_r}, \sigma_{\mathbf{y}}^2 \mathbf{I}_{N_r}\right)$, only if $\mathcal{H}_\ell \mathcal{S}_i$ is distributed according to $\mathcal{CN}\left(\mathbf{0}_{N_r}, \mathbf{I}_{N_r}\right)$. Hence, the entropy of $\mathbf{y}$ is,

$$H\left(\mathbf{y}\right) = -\mathrm{E}_{\mathbf{y}}\left\{\log_2 p_{\mathbf{y}}\left(\mathbf{y}\right)\right\} = N_r \log_2\left(\pi e\left(1 + \sigma_n^2\right)\right), \tag{14}$$

where $\sigma_{\mathbf{y}}^2 = 1 + \sigma_n^2$. Note, from [38] the entropy of an uncorrelated N–multivariate complex Normal distribution with equal variances $\left(\sigma^2\right)$ is $N \log_2\left(\pi e \sigma^2\right)$.

From (13), (26), and (14), the capacity for QSM is,

$$C = N_r \log_2\left(1 + 1/\sigma_n^2\right) = N_r \log_2\left(1 + \mathrm{SNR}\right). \tag{15}$$

In literature the capacity of SMT is [30–35],

$$C_{\text{H Dependent}} = \mathrm{E}_{\mathbf{H}}\left\{\log_2\left|\mathbf{I}_{N_r} + \frac{1}{\sigma_n^2}\mathbf{h}\mathbf{h}^H\right|\right\}. \tag{16}$$

Comparing both formulas (15) and (16), the following can be stated: 1) With proper shaping of the constellation symbols for each specific channel, QSM can achieve the theoretical channel capacity even though it has only one data stream; 2) With the proper design of the constellation symbols, the QSM capacity does *not* depend on the channel response $\mathbf{H}$, nor on the constellation symbols used, and only depends on the SNR and the number of receive antennas.

The importance of the derived capacity in (15) is demonstrated in Fig. 1, where the derived capacity in (15) is compared to the channel dependent capacity in literature in (16) for $N_t = N_r = 4$. It can be clearly seen from the figure that (16) anticipates different capacity for each channel and they all fall below the capacity given by (15). As illustrated in Fig. 1, the derived capacity shows that QSM can actually achieve 4 bits more than what is thought in literature for Rayleigh channel, 8 bits more for Rician and the 3D mmWave channel, and 11 bits more for Nakagami–m. To achieve this capacity, special design should be considered as will be discussed in the next section.

The mutual information for QSM system over mmWave, Rician, and Rayleigh fading channels with $N_r = 2$ and 4, $M = 16$–QAM, and $N_t = 2, 4$, and 8 is studied and results are depicted in Figs. 2 and 3. The Rayleigh fading channel is shown to achieve the best performance as it represents the lowest spatial correlation environment with good scattering and no LOS path. The presence of LOS path increases the spatial correlation and deteriorates the performance, which explains the inferior performance over Rician fading channel. The performance over mmWave channel is shown to lie in between Rayleigh and Rician fading channels. Please note

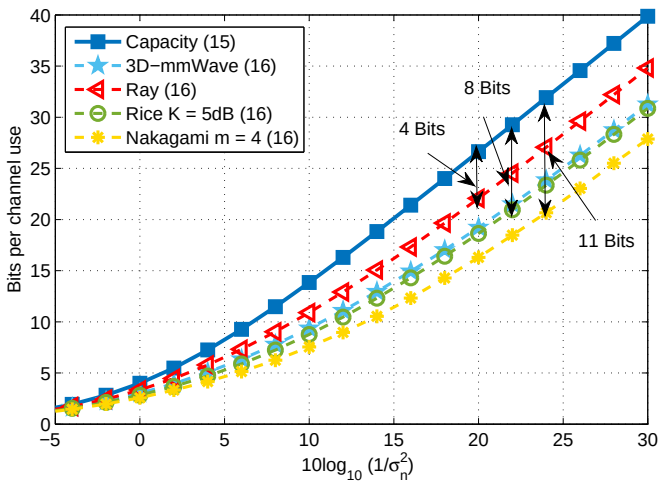

Fig. 1. Comparison between the derived capacity in (15) and the capacity derived in literature (16), for $N_t = N_r = 4$.

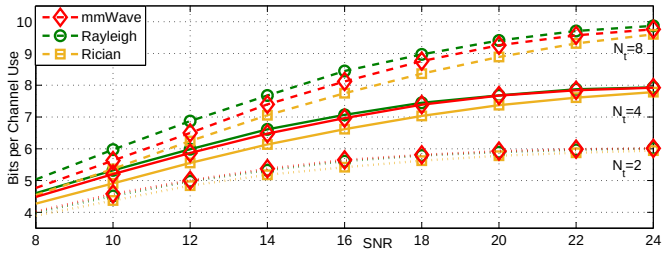

Fig. 2. Mutual information for QSM system over 3D–mmWave, Rayleigh, and Rician with $K = 5$ dB, where $N_t = 2, 4, 8$, $N_r = 2$ and QAM sysmbols used with $M = 16$.

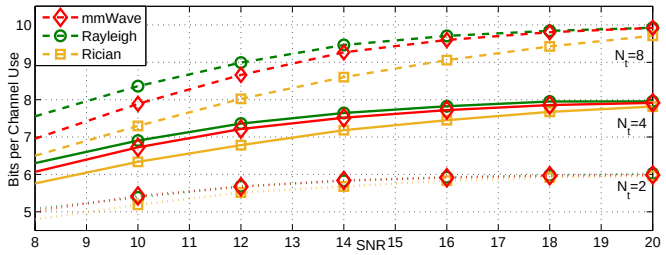

Fig. 3. Mutual information for QSM system over 3D–mmWave, Rayleigh, and Rician with $K = 5$ dB, where $N_t = 2, 4, 8$, $N_r = 4$ and QAM sysmbols used with $M = 16$.

that the small–scale spatial fading for the different multipath components in mmWave channel follow a Rician distribution as shown in [3]. However, in mmWave channel, the signal is received from different subpaths, which decreases the correlation and enhances the performance. This can be also substantiated by noting that the performance over mmWave channel enhances with increasing the number of transmit antennas and nearly approaches the Rayleigh performance with $N_t = 8$.

C. Conditions under which QSM channel Capacity can be achieved

The capacity in (15) is only achievable if each element of $\mathcal{H}_\ell \mathcal{S}_i$ follows a $\mathcal{CN}(0, 1)$. From Sec. II $\mathcal{H}_\ell \mathcal{S}_i = \mathbf{h}_{\ell^\Re} s_i^\Re + \mathbf{h}_{\ell^\Im} s_i^\Im$. Hence, for QSM system to achieve the capacity, each element of $\mathbf{h}_{\ell^\Re} s_i^\Re$ and $\mathbf{h}_{\ell^\Im} s_i^\Im$ has to follow $\mathcal{CN}(0, 1/2)$. Thus, using the product distribution theory [56], and assuming that both real and imaginary parts of the symbol s_i have the same distribution, the distribution of the used constellations has to be shaped depending on the distribution of the channel so that it solves,

$$\frac{2}{\pi} r e^{-2|r|^2} = \int \frac{1}{|h|} p_s\left(\frac{r}{h}\right) p_h(h)\, dh, \tag{17}$$

where r denotes the element wise amplitude of $\mathbf{h}_{\ell^\Re} s_i^\Re$, p_s is the PDF of the real and imaginary parts of the constellation symbols s_i, p_h is the PDF of each element of the channel $\mathbf{H}$, and h denotes the elements of $\mathbf{H}$. Therefore, constellation symbols need to be shaped for each specific channel. It should be noted though that the solution of (17) is very sophisticated and no closed–form expression is known to the authors.

The histogram of the amplitude (r_h) and the phase (ϑ_h) of the 3D mmWave channel model described in Sec. II-B are plotted in Figs. 4 and 5. From Fig. 4 it can be seen that the amplitude of the 3D mmWave channel model can be fitted to a log–normal with parameters in the range of $\mu = [-15.4086, -15.9486]$ and $\sigma = [1.19843, 1.27692]$,

$$p_{r_h}(r_h) = \frac{1}{r_h \sigma_{r_h} \sqrt{2\pi}} e^{-\frac{\left(\ln r_h - \mu_{r_h}\right)^2}{2\sigma_{r_h}^2}} \amalg_{\mathbb{R}^+}(r_h), \tag{18}$$

where $\amalg_B(b) = 1$ if $b \in B$ and zero otherwise, and $\mathbb{R}^+$ denotes the set of all positive real numbers. Furthermore, from Fig. 5 it can be seen that the phase of the 3D mmWave channel model can be fitted to a continues uniform distribution in the range of $[-\pi, \pi]$,

$$p_{\vartheta_h}(\vartheta_h) = \frac{1}{2\pi} \amalg_{[-\pi,\pi]}(\vartheta_h). \tag{19}$$

As the phase and amplitude of the 3D mmWave channel model are independent, the joint amplitude and phase PDF of the 3D mmWave channel model is,

$$p_h(h) = \frac{1}{2\pi} \frac{e^{-\frac{\left(\ln r_h - \mu_{r_h}\right)^2}{2\sigma_{r_h}^2}}}{r_h \sigma_{r_h} \sqrt{2\pi}} \amalg_{\mathbb{R}^+}(r_h) \amalg_{[-\pi,\pi]}(\vartheta_h). \tag{20}$$

Substituting (20) in (17) yields,

$$2re^{-|r|^2} = \frac{1}{\sigma_{r_h} 2\sqrt{2\pi}} \int_0^\infty \frac{1}{|h|^2} p_s\left(\frac{r}{h}\right) e^{-\frac{\left(\ln |h| - \mu_{r_h}\right)^2}{2\sigma_{r_\mathbf{h}}^2}} dh. \tag{21}$$

From (21) it can be seen that for QSM to achieve the capacity over the 3D mmWave channel, the constellation symbols have to be shaped, as in [57] for instance, such that the PDF of the constellation symbols (p_s) solves (21). It is a two stages process where in the first stage, the distribution of the constellation symbols (p_s) has to be found for the

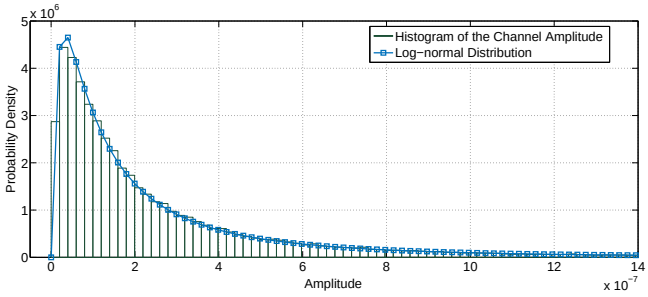

Fig. 4. Histogram of the amplitude of the 3D mmWave Channel model fitted to a log–normal distribution.

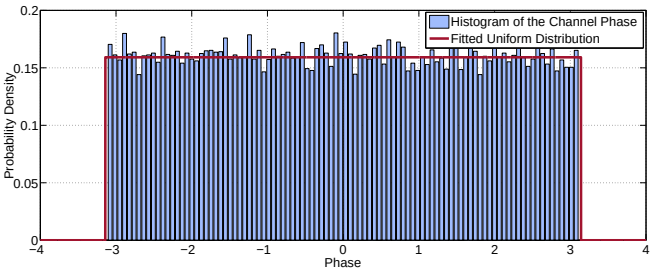

Fig. 5. Histogram of the phase of the 3D mmWave Channel model fitted to a uniform distribution.

given channel statistics (p_h) by solving (17). Substituting the mmWave channel distribution given in (20) in (17) leads to (21). Unfortunately, no closed form solution for p_s in (21) is available even with math tools such as Mathematica and Maple. However, and even if a solution was available for p_s from (21), the second stage is to shape the constellation symbols to achieve p_s. Signal shaping or other methods need to be considered to shape the constellation symbols such that their distribution follows the obtained p_s. Again, this is another design problem that is mathematically involved and requires further investigations and studies. Clearly, these issues are beyond the scope of this paper but they are very interesting topics for future research.

In almost all previous studies dealing with SM capacity over mmWave channel, as in [58, and references therein], it is concluded that signal constellation symbols must be Gaussian to achieve the theoretical capacity, see theorem I just above (30) in [58]. However, it is shown in what follows that the complex Gaussian distribution is not the needed distribution to achieve the theoretical capacity, and to achieve the capacity p_s should be obtained from (17), or in the case of the 3D mmWave channel model used in this paper from (21). In Fig. 6, the mutual information for a QSM system over 3D–mmWave channel with $N_t = 8$, $N_r = 2$ and $M = 1024$ constellation size is computed assuming Gaussian distributed symbols and QAM symbols. As can be clearly seen from the figure that even with the assumption of Gaussian distributed symbols, the achieved mutual information is 0.5 bits less than what QAM symbols achieved. Clearly, Gaussian distribution is not the required distribution to achieve the theoretical capacity. The theoretical capacity is far away and requires proper design of the constellation symbols for the specific nature of the channel distribution.

IV. Results

Monte Carlo simulations are conducted to study the capacity performance of mmWave–QSM system. Furthermore, a log-normal fitting for the 3D mmWave empirical channel model in [3] is considered and capacity and ABER performance are studied. In all results, the carrier frequency is $f = 73$ GHz.

The closed–form capacity of QSM derived in (15), along with the mutual information simulation results of QSM for $\eta = 6, 8, 10, 12,$ and 14 bits over an $N_t = N_r = 2$, $N_t = 2$ and $N_r = 4$, $N_t = 4$ and $N_r = 2$, and $N_t = N_r = 4$ mmWave channels are shown in Figs. 7- 10, respectively. In the Figs. 7- 10, mutual information curves for the different spectral efficiencies are shown to follow the theoretical capacity closely until a spectral efficiency of about 4 bits. This validates the capacity bound derived in (15), and confirms that QSM can achieve the theoretical capacity limit.

However, for spectral efficiencies larger than 4 bits, mutual information curves deviate from the capacity curve. The reason for this is discussed before in Section III-C. To achieve the channel capacity, the probability distribution of $\mathbf{Hx}$ has to be a complex normal distribution. In other words, (17) should be solved for p_s and signal shaping should be considered such that the distribution of the constellation symbols is p_s.

Figs. 7- 10 also depict the mutual information results of QSM over lognormal fading channels with uniformly distributed phase. The mutual information results for the 3D mmWave channel and for the lognormal fading channel demonstrate close match for wide and pragmatic range of SNR values and for different number of transmit and receive antennas. Furthermore, Fig. 11 depicts the ABER performance of QSM over both the 3D mmWave channel model and the lognormal fading channel model for $\eta = 10$ and $N_t = N_r = 2, 4,$ and 8. It can be seen that the ABER performance results for QSM over the lognormal fading channel closely follow that over the 3D mmWave channel. These results along with the discussion in Sec. III-B, validates that the 3D mmWave channel model in [3] can be closely approximated by a log-normal fading channel with uniform phase distribution.

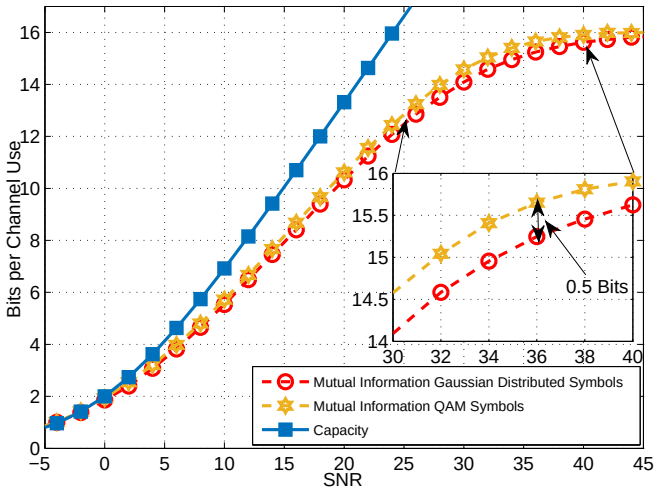

Fig. 6. Mutual information for a QSM system over 3D–mmWave channel with $N_t = 8$, $N_r = 2$ and $M = 1024$ constellation diagram assuming Gaussian distributed symbols and QAM symbols.

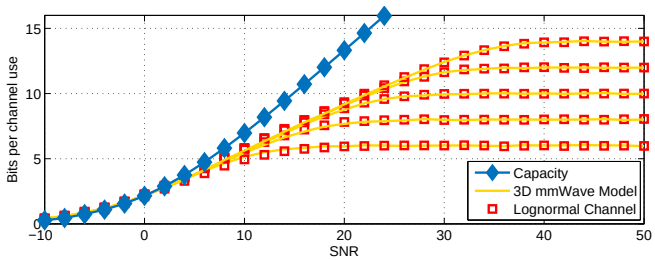

Fig. 7. Capacity and simulated mutual information of mmWave–QSM with $\eta = 6, 8, 10, 12,$ and 14, $N_t = N_r = 2$.

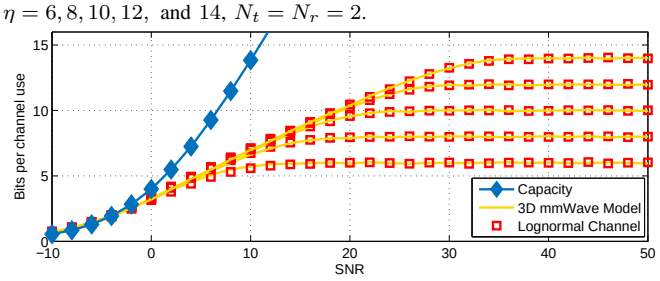

Fig. 8. Capacity and simulated mutual information of mmWave–QSM with $\eta = 6, 8, 10, 12,$ and 14, $N_t = 2, N_r = 4$.

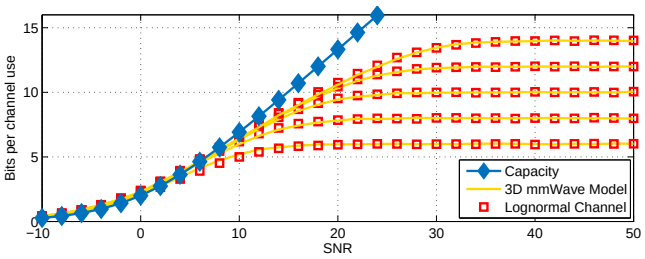

Fig. 9. Capacity and simulated mutual information of mmWave–QSM with $\eta = 6, 8, 10, 12,$ and 14, $N_t = 4, N_r = 2$.

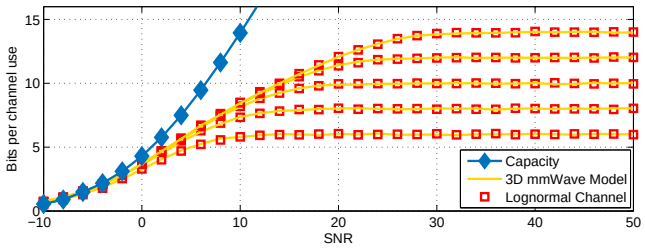

Fig. 10. Capacity and simulated mutual information of mmWave–QSM with $\eta = 6, 8, 10, 12,$ and 14, $N_t = N_r = 4$.

Finally, QSM performance is compared to SM and spatial multiplexing (SMX) [59] systems over the 3D mmWave channel model for $\eta = 8$ and 12, and $N_t = N_r = 4$. The derived capacity for QSM in (15) along with simulation results of the mutual information for QSM, SM, and SMX systems over the 3D mmWave channel model are depicted in Fig. 12. It can be seen that QSM outperforms SM for both $\eta = 8$ and 12, and offers the same performance as SMX for $\eta = 8$. However, for larger spectral efficiency, $\eta = 12$, SMX outperforms QSM by about 0.8 bit. This enhancement can be attributed due to the need of smaller constellation diagram of SMX as compared to QSM. Please note that for $\eta = 8$, SMX constellation size is 75% smaller than that of the QSM constellation. Whereas for $\eta = 12$, SMX constellation size is about 97% smaller than the QSM constellation size.

It should be noted though that all depicted results perform much less than the anticipated theoretical capacity of QSM system. As discussed earlier, proper design of the signal constellation for the specific nature of the considered channel is needed to achieve this capacity. It should be also mentioned that even though QSM and SM need larger constellation diagram than SMX, they offer huge energy saving potentials [60], and large reduction in computational complexity [61].

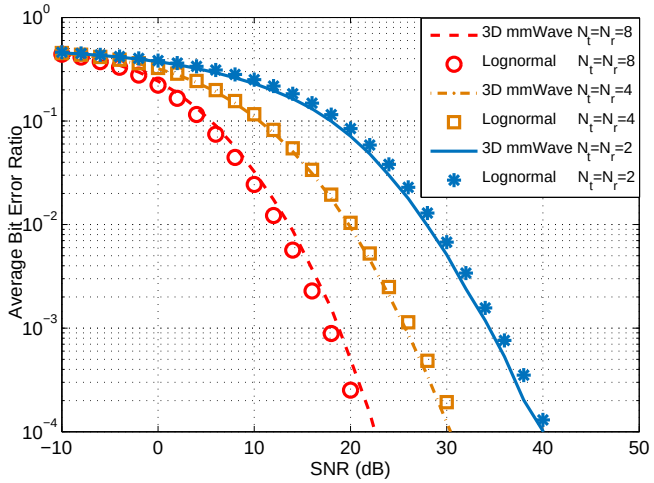

Fig. 11. ABER of 3D-mmWave–QSM with $\eta = 10$, $N_t = N_r = 2, 4,$ and 8.

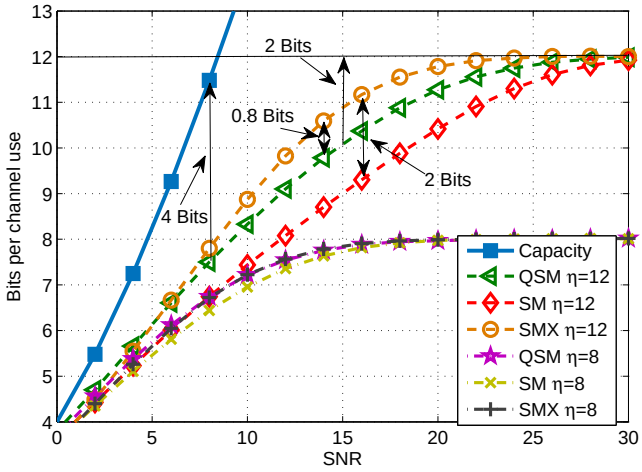

Fig. 12. The capacity of QSM compared to the simulated mutual information of QSM, SM, and SMX over the 3D–mmWave channel model, for $\eta = 8,$ and 12, and $N_t = N_r = 4$.

V. Conclusions

Capacity analysis for QSM MIMO system over mmWave channels is studied in this paper. The mutual information and the capacity are derived and the conditions under which channel capacity can be achieved are derived and discussed. It is shown that QSM system can achieve the channel capacity with only single data stream. This is in contrast to other spatial multiplexing systems, where channel capacity can be achieved if the number of available data streams equal the minimum number among transmit and receive antennas. Obtained results reveal that the QSM capacity can be attained by shaping the constellation symbols based on the distribution of the channel, such that the resultant of the constellation symbol passing through the channel follows a complex Gaussian distribution. Such design and constellation shaping will be the subject of future research. With proper design, QSM can theoretically achieve higher capacity than that of SMX system. It is also shown that the 3D outdoor mmWave channel model can be closely fitted with a log–normal fading channel. The formula to design the constellation symbols for QSM system over mmWave channel is derived and shown to be mathematically involved. Hence, it is left for future investigations.

Appendix A
Derrivation of $I(\mathcal{H}_\ell, \mathcal{S}_i; \mathbf{y})$ in (12)

Firstly, derive $H(\mathbf{y})$,

$$\begin{aligned} H(\mathbf{y}) &= -\int_{\mathbf{y}} p_{\mathbf{y}}(\mathbf{y}) \log_2 p_{\mathbf{y}}(\mathbf{y})\, dy \\ &= -\mathrm{E}_{\mathbf{y}}\left\{\log_2 p_{\mathbf{y}}(\mathbf{y})\right\}, \end{aligned} \tag{22}$$

where $p_{\mathbf{y}}(\cdot)$ is the PDF of the received vector $\mathbf{y}$,

$$p_{\mathbf{y}} = \int_{\mathcal{H}_\ell,\mathcal{S}_i} p_{\mathcal{H}_\ell}(\mathcal{H}_\ell)\, p_{\mathcal{S}_i}(\mathcal{S}_i)\, p_{(\mathbf{y}|\mathcal{H}_\ell,\mathcal{S}_i)}(\mathbf{y}|\mathcal{H}_\ell,\mathcal{S}_i)\; d\mathcal{H}_\ell\, d\mathcal{S}_i$$
$$= \frac{1}{(\pi\sigma_n^2)^{N_r}} \mathrm{E}_{\mathcal{H}_\ell,\mathcal{S}_i}\left\{ e^{\frac{-\|\mathbf{y}-\mathcal{H}_\ell\mathcal{S}_i\|_{\mathrm{F}}^2}{\sigma_n^2}} \right\}, \quad (23)$$

where $p_{(\mathbf{y}|\mathcal{H}_\ell,\mathcal{S}_i)}$ is the PDF of the received vector $\mathbf{y}$ knowing the spatial and constellation symbols, $\mathcal{H}_\ell$ and $\mathcal{S}_i$ respectively, and it is given by,

$$p_{(\mathbf{y}|\mathcal{H}_\ell,\mathcal{S}_i)}(\mathbf{y}|\mathcal{H}_\ell,\mathcal{S}_i) = \frac{1}{(\pi\sigma_n^2)^{N_r}} e^{\frac{-\|\mathbf{y}-\mathcal{H}_\ell\mathcal{S}_i\|_{\mathrm{F}}^2}{\sigma_n^2}}. \quad (24)$$

From (22) and (23), the entropy of $\mathbf{y}$ is,

$$H(\mathbf{y}) = N_r \log_2\left(\pi\sigma_n^2\right) - \mathrm{E}_{\mathbf{y}}\left\{ \log_2\left(\mathrm{E}_{\mathcal{H}_\ell,\mathcal{S}_i}\left\{ e^{\frac{-\|\mathbf{y}-\mathcal{H}_\ell\mathcal{S}_i\|_{\mathrm{F}}^2}{\sigma_n^2}} \right\} \right) \right\}. \quad (25)$$

Secondly, the entropy of $\mathbf{y}$ knowing $\mathcal{H}_\ell, \mathcal{S}_i$ is,

$$H(\mathbf{y}|\mathcal{H}_\ell,\mathcal{S}_i) = -\mathrm{E}_{\mathbf{y}}\left\{\log_2 p_{\mathbf{y}|\mathcal{H}_\ell,\mathcal{S}_i}(\mathbf{y}|\mathcal{H}_\ell,\mathcal{S}_i)\right\}$$
$$= -\mathrm{E}_{\mathbf{n}}\left\{\log_2 p_{\mathbf{n}}(\mathbf{n}+\mathcal{H}_\ell\mathcal{S}_i)\right\}$$
$$= N_r \log_2\left(\pi\sigma_n^2 e\right), \quad (26)$$

where $p_{\mathbf{n}}$ is the PDF of the noise vector $\mathbf{n}$. Note, from [38] the entropy of an N length complex Guassian random vector with mean u and variance σ^2 is $N\log_2(\pi\sigma^2 e)$.

Finally, substituting (25) and (26), in (11) lead to $I(\mathcal{H}_\ell, \mathcal{S}_i; \mathbf{y})$ given in (12).

REFERENCES

[1] Z. Pi and F. Khan, "An Introduction to Millimeter-Wave Mobile Broadband Systems," *IEEE Commun. Mag.*, vol. 49, no. 6, pp. 101–107, Jun. 2011.

[2] T. Rappaport, S. Sun, R. Mayzus, H. Zhao, Y. Azar, K. Wang, G. Wong, J. Schulz, M. Samimi, and F. Gutierrez, "Millimeter Wave Mobile Communications for 5G Cellular: It Will Work!" *IEEE Access*, vol. 1, pp. 335–349, 2013.

[3] M. K. Samimi and T. S. Rappaport, "3-D Millimeter-Wave Statistical Channel Model for 5G Wireless System Design," *IEEE Trans. Microw. Theory Techn.*, vol. 64, no. 7, pp. 2207–2225, July 2016.

[4] J. Wells, "Faster than fiber: The future of multi-G/s wireless," *IEEE Microw. Mag.*, vol. 10, no. 3, pp. 104–112, May 2009.

[5] ——, "Multigigabit wireless technology at 70 GHz, 80 GHz and 90 GHz," *RF Design*, pp. 50–58, May 2006.

[6] S. Nie, G. R. MacCartney, S. Sun, and T. S. Rappaport, "72 GHz Millimeter Wave Indoor Measurements for Wireless and Backhaul Communications," in *IEEE 24th Annual Int. Symp. on Pers., Indoor and Mobile Radio Commun. (PIMRC)*, Sep. 2013, pp. 2429–2433.

[7] G. R. MacCartney and T. S. Rappaport, "73 GHz Millimeter Wave Propagation Measurements for Outdoor Urban Mobile and Backhaul Communications in New York City," in *IEEE Int. Conf. on Commun. (ICC)*, Jun. 2014, pp. 4862–4867.

[8] *Characteristics of Percipitation for Propagation Modeling*, ITU-R Std. P.837-4, 2003.

[9] *mmWave WPAN (IEEE 802.15.3c-2009)*, IEEE Std., Oct. 2009, Amendment to IEEE Std 802.15.3-2003.

[10] *WiGig (IEEE 802.11ad)*, IEEE Std., Dec. 2012.

[11] *WirelessHD*, Std., May 2010. [Online]. Available: http://www.wirelesshd.org/

[12] Q. Li, G. Li, W. Lee, M. il Lee, D. Mazzarese, B. Clerckx, and Z. Li, "MIMO techniques in WiMAX and LTE: A Feature Overview," *IEEE Commun. Mag.*, vol. 48, no. 5, pp. 86 –92, May 2010.

[13] J. Mietzner, R. Schober, L. Lampe, W. H. Gerstacker, and P. A. Höeher, "Multiple-Antenna Techniques for Wireless Communications - A Comprehensive Literature Survey," *IEEE Commun. Surveys Tuts.*, vol. 11, no. 2, pp. 87 –105, 2009.

[14] Y. A. Chau and S.-H. Yu, "Space Modulation on Wireless Fading Channels," in *IEEE Vehicular Technology Conference (VTC Fall 2001)*, vol. 3, 7–11 Oct. 2001, pp. 1668–1671.

[15] E. Basar, "Index modulation techniques for 5G wireless networks," *IEEE Commun. Mag.*, vol. 54, no. 7, pp. 168–175, Jul. 2016.

[16] M. Di Renzo, H. Haas, A. Ghrayeb, S. Sugiura, and L. Hanzo, "Spatial Modulation for Generalized MIMO: Challenges, Opportunities, and Implementation," *Proc. of the IEEE*, vol. 102, no. 1, pp. 56–103, Jan 2014.

[17] N. Serafimovski, A. Younis, and H. Haas, "Spatial Modulation," Oct. 2012. [Online]. Available: http://youtu.be/cPKIbxrEDho

[18] Y. Bian, X. Cheng, M. Wen, L. Yang, H. V. Poor, and B. Jiao, "Differential Spatial Modulation," *IEEE Trans. on Veh. Technol.*, vol. 64, no. 7, pp. 3262–3268, Jul. 2015.

[19] M. Wen, X. Cheng, Y. Bian, and H. V. Poor, "A Low-Complexity Near-ML Differential Spatial Modulation Detector," *IEEE Signal Process. Lett.*, vol. 22, no. 11, pp. 1834–1838, Nov. 2015.

[20] M. Zhang, M. Wen, X. Cheng, and L. Yang, "A Dual-Hop Virtual MIMO Architecture Based on Hybrid Differential Spatial Modulation," *IEEE Trans. on Wireless Commun.*, vol. 15, no. 9, pp. 6356–6370, Sep. 2016.

[21] A. Younis, N. Serafimovski, R. Mesleh, and H. Haas, "Generalised Spatial Modulation," in *Asilomar Conf. on Signals, Systems, and Computers*, Pacific Grove, CA, USA, Nov. 2010.

[22] A. Younis, R. Mesleh, M. D. Renzo, and H. Haas, "Generalised Spatial Modulation for Large–Scale MIMO," in *Proc. of the 22nd European Signal Processing Conf. (EUSIPCO)*, Lisbon, Portugal, Sep. 1-5 2014.

[23] R. Mesleh, S. S. Ikki, and H. M. Aggoune, "Quadrature Spatial Modulation System," U.S. Patent 61/897,894, October 31, 2013.

[24] R. Mesleh, S. Ikki, and H. Aggoune, "Quadrature Spatial Modulation," *IEEE Trans. Veh. Technol.*, vol. 64, no. 6, pp. 2738–2742, Jun. 2015.

[25] R. Mesleh, H. Haas, S. Sinanović, C. W. Ahn, and S. Yun, "Spatial Modulation," *IEEE Trans. on Veh. Tech.*, vol. 57, no. 4, pp. 2228 – 2241, Jul. 2008.

[26] J. Jeganathan, A. Ghrayeb, L. Szczecinski, and A. Ceron, "Space Shift Keying Modulation for MIMO Channels," *IEEE Trans. on Wireless Commun.*, vol. 8, no. 7, pp. 3692–3703, Jul. 2009.

[27] R. Mesleh, S. S. Ikki, and el Hadi M. Aggoune, "Quadrature Spatial Modulation–Performance Analysis and Impact of Imperfect Channel Knowledge," *Trans. on Emerging Telecommun. Technol.*, vol. 28, no. 1, 2014.

[28] A. Younis, R. Mesleh, and H. Haas, "Quadrature Spatial Modulation Performance over Nakagami–m Fading Channels," *IEEE Trans. on Veh. Technol.*, vol. 65, no. 12, pp. 10 227–10 231, Dec. 2015.

[29] B. Zheng, F. Chen, M. Wen, F. Ji, H. Yu, and Y. Liu, "Low-Complexity ML Detector and Performance Analysis for OFDM With In-Phase/Quadrature Index Modulation," *IEEE Commun. Lett.*, vol. 19, no. 11, pp. 1893–1896, Nov 2015.

[30] D. Basnayaka and H. Haas, "Spatial Modulation for Massive MIMO," in *Proc. of IEEE Int. Conf. on Commun. (ICC)*, Jun. 2015, pp. 1945–1950.

[31] Y. Yang and B. Jiao, "Information-Guided Channel-Hopping for High Data Rate Wireless Communication," *IEEE Commun. Lett.*, vol. 12, no. 4, pp. 225 –227, Apr. 2008.

[32] ——, "On the Capacity of Information-Guided Channel-Hopping in Multi-Antenna System," in *IEEE INFOCOM Workshops 2008*, Apr. 2008, pp. 1–5.

[33] H. Yonghong, W. Pichao, W. Xiang, Z. Xiaoming, and H. Chunping, "Ergodic Capacity Analysis of Spatially Modulated Systems," *China Commun.*, vol. 10, no. 7, pp. 118–125, Jul. 2013.

[34] A. Younis, D. A. Basnayaka, and H. Haas, "Performance Analysis for Generalised Spatial Modulation," in *Proc. of European Wireless Conf. (EW 2014)*, Barcelona, Spain, 14–16 May 2014, pp. 207–212.

[35] N. Ishikawa, R. Rajashekar, S. Sugiura, and L. Hanzo, "Generalized Spatial Modulation Based Reduced-RF-Chain Millimeter-Wave Communications," *IEEE Trans. Veh. Technol.*, vol. 66, no. 1, pp. 879–883, Jan. 2017.

[36] A. Younis, "Spatial Modulation: Theory to Practice," Ph.D. dissertation, University of Edinburgh, Edinbrugh, UK, 2014.

[37] L. Zheng and D. N. Tse, "Diversity and Multiplexing: A Fundamental Tradeoff in Multiple-Antenna Channels," *IEEE Trans. on Inform. Theory*, vol. 49, no. 5, pp. 1073–1096, May 2003.

[38] E. Telatar, "Capacity of Multi-Antenna Gaussian Channels," *European Trans. on Telecommun.*, vol. 10, no. 6, pp. 585–595, Nov. / Dec. 1999.

[39] J. Ahmadi-Shokouh, R. Rafi, A. Taeb, and S. Safavi-Naeini, "Empirical MIMO Beamforming and Channel Measurements at 5764GHz Frequencies," *Trans. on Emerg. Telecommun. Technol.*, vol. 26, no. 6, pp. 1003–1009, 2015.
[40] A. Maltsev, A. Sadri, C. Cordeiro, and A. Pudeyev, "Practical LOS MIMO Technique for Short-Range Millimeter-Wave Systems," in *IEEE Intern. Conf. on Ubiquitous Wireless Broadband (ICUWB)*, Oct 2015, pp. 1–6.
[41] E. Torkildson, H. Zhang, and U. Madhow, "Channel Modeling for Millimeter Wave MIMO," in *Inf. Theory and Appl. Workshop (ITA)*, Jan. 2010, pp. 1–8.
[42] S. T. Shah, J. S. Kim, E. S. Bae, J. Bae, and M. Y. Chung, "Radio Resource Management for 5G Mobile Communication Systems with Massive Antenna Structure," *Trans. on Emerg. Telecommun. Technol.*, vol. 27, no. 4, pp. 504–518, 2016.
[43] E. Torkildson, U. Madhow, and M. Rodwell, "Indoor Millimeter Wave MIMO: Feasibility and Performance," *IEEE Trans. Wireless Commun.*, vol. 10, no. 12, pp. 4150–4160, Dec. 2011.
[44] L. Zhou and Y. Ohashi, "Performance Analysis of mmWave LOS-MIMO Systems with Uniform Circular Arrays," in *IEEE 81st Veh. Technol. Conf. (VTC Spring)*, May 2015, pp. 1–5.
[45] P. Liu and A. Springer, "Space Shift Keying for LOS Communication at mmWave Frequencies," *IEEE Wireless Commun. Lett.*, vol. 4, no. 2, pp. 121 –124, Apr. 2015.
[46] T. A. Thomas, H. C. Nguyen, G. R. MacCartney, and T. S. Rappaport, "3D mmWave Channel Model Proposal," in *IEEE 80th Veh. Technol. Conf. (VTC Fall)*, Sept 2014, pp. 1–6.
[47] M. K. Samimi, S. Sun, and T. S. Rappaport, "MIMO Channel Modeling and Capacity Analysis for 5G Millimeter-Wave Wireless Systems," in *10th European Conference on Antennas and Propagation (EuCAP2016)*, Apr. 2016.
[48] M. K. Samimi and T. S. Rappaport, "3-D Statistical Channel Model for Millimeter-Wave Outdoor Mobile Broadband Communications," in *In the Proceeding of the IEEE Intern. Conf. on Commun.* , Jun. 8–12, 2015.
[49] M. Steinbauer, A. F. Molisch, and E. Bonek, "The Double-Directional Radio Channel," *IEEE Antennas and Propag. Mag.*, vol. 43, no. 4, pp. 51–63, Aug. 2001.
[50] A. Forenza, D. J. Love, and R. W. Heath, "Simplified Spatial Correlation Models for Clustered MIMO Channels With Different Array Configurations," *IEEE Trans. on Veh. Technol.*, vol. 56, no. 4, pp. 1924–1934, Jul. 2007.
[51] A. F. Molisch, M. Steinbauer, M. Toeltsch, E. Bonek, and R. S. Thoma, "Capacity of MIMO Systems Based on Measured Wireless Channels," *IEEE J. Sel. Areas Commun.*, vol. 20, no. 3, pp. 561–569, Apr. 2002.
[52] R. Mesleh, "Spatial Modulation: A Spatial Multiplexing Technique for Efficient Wireless Data Transmission," Ph.D. dissertation, Jacobs University, Bremen, Germany, Jun. 2007.
[53] P. Karttunen, K. Kalliola, T. Laakso, and P. Vainikainen, "Measurement Analysis of Spatial and Temporal Correlation in Wideband Radio Channels with Adaptive Antenna Array," in *IEEE 1998 Intern. Conf. on Universal Personal Commun. (ICUPC '98)*, vol. 1, Oct 1998, pp. 671–675 vol.1.
[54] V. Kühn, *Wireless Communications over MIMO Channels*. John Wiley & Sons Ltd., 2006.
[55] C. Shannon, "A Mathematical Theory of Communication," *Bell System Technical Journal*, vol. 27, pp. 379–423 & 623–656, Jul. & Oct. 1948.
[56] G. R. Grimmett and D. R. Stirzaker, *Probability and Random Processes*, 3rd ed. Oxford University Press, Aug. 2001.
[57] A. Calderbank and L. Ozarow, "Nonequiprobable Signaling on The Gaussian Channel," *IEEE Trans. Inf. Theory*, vol. 36, no. 4, pp. 726–740, Jul. 1990.
[58] P. Liu, M. D. Renzo, and A. Springer, "Line-of-Sight Spatial Modulation for Indoor mmWave Communication at 60 GHz," *IEEE Trans. Wireless Commun.*, vol. 15, no. 11, pp. 7373–7389, Nov. 2016.
[59] G. J. Foschini, "Layered Space-Time Architecture for Wireless Communication in a Fading Environment when Using Multi-Element Antennas," *Bell Labs Tech. J.*, vol. 1, no. 2, pp. 41–59, 1996.
[60] A. Stavridis, S. Sinanović, M. D. Renzo., and H. Haas, "Energy Evaluation of Spatial Modulation at a Multi-Antenna Base Station," in *Proc. of the 78th IEEE Veh. Tech. Conf. (VTC)*, Las Vegas, USA, Sep. 2–5, 2013.
[61] A. Younis, S. Sinanovic, M. Di Renzo, R. Mesleh, and H. Haas, "Generalised Sphere Decoding for Spatial Modulation," *IEEE Trans. on Commun.*, vol. 61, no. 7, pp. 2805–2815, 2013.

Abdelhamid Younis is currently the head of the Electrical and Electronics Engineering Department at the University of Benghazi, Libya, where he joined the department in 2015. He received the B.Sc. (with honors) in 2007 from the University of Benghazi, and the M.Sc. (with distinction) and Ph.D. in 2009 and 2013, respectively, from The University of Edinburgh, U.K.. He was a research associate at the Institute of Digital Communications at the University of Edinburgh from 2013 to 2014. Dr. Younis received the Overseas Research Student Award in 2010, best student paper award at the 78th IEEE Vehicular Technology Conference (VTC) in Las Vegas, Sep. 2013, the Graphical System Design Achievement Awards Category: Radio Frequency (RF) and Communications from National Instruments (NI), and holds the Almadar Aljadid R&D grant titled "Millimeter–Wave Large–Scale MIMO: ABER and Capacity Analysis".

Nagla Abuzgaia is a faculty member at the Electrical and Electronics Engineering Department at the University of Benghazi since 2010. She received the B.Sc. and M.Sc. degrees in Electrical and Electronics Engineering (with honors) in 2007 and 2010 respectively, from the University of Benghazi, Libya. She was a teaching assistant engineer in the Electrical Engineering Department at the University of Benghazi from 2007 to 2010. Her research interests focus on wireless communications and internet of things (IoT).

Raed Mesleh is currently the vice dean of the school of electrical engineering and information technology at German Jordanian University in Amman, Jordan. He received his Ph.D. in 2007 from Jacobs University in Bremen, Germany. From 2007 to 2010 he was a postdoctoral fellow at Jacobs University. He was with the Electrical Engineering Department at University of Tabuk in Saudi Arabia from 2010 to 2015. During that period, he holds the position of department chair and the director of research excellence and intellectual property units at the deanship of scientific research. He was a visiting scholar at Boston University, The University of Edinburgh and HerriotWatt University. In December 2016, he was awarded the Arab Scientific Creativity award from Arab Thought Foundation.

Harald Haas (S98A00M03-SM16) currently holds the Chair of Mobile Communications with The University of Edinburgh. He is also a co-founder and the Chief Scientific Officer of pureLiFi Ltd., as well as the Director of the LiFi Research and Development Center, The University of Edinburgh. His main research interests are in optical wireless communications, hybrid optical wireless and RF communications, spatial modulation, and interference coordination in wireless networks. He first introduced and coined spatial modulation and LiFi. LiFi was listed among the 50 best inventions in Time magazine in 2011. In 2014, he was selected by EPSRC as one of ten RISE (Recognising Inspirational Scientists and Engineers) Leaders in the U.K, and received the Outstanding Achievement Award from the International Solid State Lighting Alliance (ISA) in 2016.